Finally, substituting (16.14) in (16.10), we obtain

$$U_o(\tilde{\rho}_2) = \sqrt{\frac{P_t}{\pi a^2(L)}}\, \exp[jkL + j\Theta(L)]\, \exp[jk|\tilde{\rho}_2|^2/2q(L)], \tag{16.16}$$

explicitely showing that a Gaussian beam maintains its form as it propagates through free-space. At $z = L$, the field $U_o(\tilde{\rho}_2)$ is properly normalized. This is evidenced by the correct intensity radius $a(L)$ entering the normalization factor $\sqrt{P_t/\pi a^2(L)}$. From Eq. (16.5), it is clear then that the total power crossing the $z = L$ plane is still given by P_t. This should be expected because we are talking about Gaussian beams propagating in free space.

16.3 Paraxial Helmholtz Equation

We pointed out at the beginning of Sec. 16.2 that Gaussian beams satisfy the Fresnel diffraction formula (15.12) which applies under paraxial conditions. The latter can be thought of as the integral form of the Helmholtz Eq. (13.3) after paraxial approximation has been applied to it. Here we derive this paraxial form of the Helmholtz equation. We will leave the proof that a Gaussian beam described by Eq. (16.2) satisfies the paraxial Helmholtz equation as a homework exercise.

Substituting (16.1) in the Helmholtz Eq. (13.3), we obtain

$$(\nabla_t^2 + \frac{\partial^2}{\partial z^2}) U_z(\tilde{\rho}) \exp(jkz) + k^2\, U_z(\tilde{\rho})\, \exp(jkz) = 0,$$

where $\nabla_t^2 \equiv \dfrac{\partial^2}{\partial x^2} + \dfrac{\partial^2}{\partial y^2}$, and we have explicitely noted the implicit dependence of $U(\tilde{\rho})$ on z [via $a(z)$ and $R(z)$] by subscripting the former. The above equation is easily simplified to

$$\nabla_t^2 U_z(\tilde{\rho}) + \frac{\partial^2}{\partial z^2} U_z(\tilde{\rho}) + 2jk \frac{\partial}{\partial z} U_z(\tilde{\rho}) = 0. \tag{16.17}$$

The paraxial approximation is now applied by neglecting $\dfrac{\partial^2 U_z}{\partial z^2}$ as compared with $k\dfrac{\partial U_z}{\partial z} \sim \dfrac{1}{\lambda}\dfrac{\partial U_z}{\partial z}$. Physically, it says that the change in $\dfrac{\partial U_z}{\partial z}$ along z is negligibly small over a wavelength. Throwing away the middle term on the left side of Eq. (16.17), we obtain

$$\nabla_t^2 U_z(\tilde{\rho}) + 2jk \frac{\partial}{\partial z} U_z(\tilde{\rho}) = 0, \tag{16.18}$$

which is known as the *paraxial Helmholtz equation*. It can be shown, with little effort, that the Fresnel diffraction formula is an exact solution of the above equation for an arbitrary input field $U_i(\bar{\rho}_1)$.

16.4 Elliptic Gaussian Beams

The Gaussian beam defined by Eq. (16.2) is cylindrically symmetric. The intensity radius a and the phase radius of curvature R are the same along both x and y directions. Many optical systems, however, are not cylindrically symmetric. In such systems, more general forms of Gaussian beams can exist. We first generalize to the case of an elliptic Gaussian beam defined by the following transverse spatial dependence:

$$U(\bar{\rho}) = \sqrt{\frac{P_t}{\pi a_x a_y}} \exp\left(jkx^2/2q_x\right) \exp\left(jky^2/2q_y\right), \tag{16.19}$$

where

$$\frac{1}{q_x} = \frac{1}{R_x} + \frac{j}{ka_x^2}, \quad \text{and} \quad \frac{1}{q_y} = \frac{1}{R_y} + \frac{j}{ka_y^2}. \tag{16.20}$$

Taking the modulus square of Eq. (16.19), the intensity profile is given by

$$I(\bar{\rho}) = |U(\bar{\rho})|^2 = \frac{P_t}{\pi a_x a_y} \exp\left(-x^2/a_x^2\right) \exp\left(-y^2/a_y^2\right). \tag{16.21}$$

From the above equation, we identify a_x to be the intensity radius along the x direction and a_y to be that along the y direction. Similarly, by looking at the phase part of Eq. (16.19), we identify R_x to be the phase radius of curvature along the x direction and R_y to be that along the y direction. Integrating $I(\bar{\rho})$ over the x-y plane, one can verify that the total power carried by the beam is P_t.

Following steps similar to those in Eqs. (16.6)-(16.11), we now show that an elliptic Gaussian beam stays elliptic as it propagates through free space. In the input plane at $z = 0$, the Fourier transform of the elliptic Gaussian beam is

$$\tilde{U}_i(\bar{f}) = \sqrt{\frac{P_t}{\pi a_{x0} a_{y0}}} \sqrt{j\lambda q_{x0}} \sqrt{j\lambda q_{y0}} \exp\left(-j\pi\lambda q_{x0} f_x^2\right) \exp\left(-j\pi\lambda q_{y0} f_y^2\right), \tag{16.22}$$

where the subscript 0 specifies the parameters a_{x0}, a_{y0}, q_{x0}, and q_{y0} in the $z = 0$ plane. Using Eqs. (15.7) and (15.9), the Fourier transform of the output field at $z = L$ is given by

$$\begin{aligned}\tilde{U}_o(\bar{f}) &= \sqrt{\frac{P_t}{\pi a_{x0} a_{y0}}}\sqrt{j\lambda q_{x0}}\sqrt{j\lambda q_{y0}}\exp(jkL) \\ &\quad \times \exp\left[-j\pi\lambda(q_{x0}+L)f_x^2\right]\exp\left[-j\pi\lambda(q_{y0}+L)f_y^2\right] \\ &= \sqrt{\frac{P_t}{\pi a_{x0} a_{y0}}}\sqrt{\frac{q_{x0}}{q_x(L)}}\sqrt{\frac{q_{y0}}{q_y(L)}}\exp(jkL) \\ &\quad \times\sqrt{j\lambda q_x(L)}\sqrt{j\lambda q_y(L)}\exp\left[-j\pi q_x(L)f_x^2\right]\exp\left[-j\pi q_y(L)f_y^2\right] \qquad (16.23)\end{aligned}$$

where

$$q_x(L) = q_{x0} + L, \quad \text{and} \quad q_y(L) = q_{y0} + L. \qquad (16.24)$$

Thus, as the elliptic Guassian beam propagates in free space, its parameters q_x and q_y independently change in the same way as the parameter q for the circularly-symmetric Gaussian beam. Inverse Fourier transforming Eq. (16.23), we obtain

$$\begin{aligned}U_o(\bar{\rho}_2) &= \sqrt{\frac{P_t}{\pi a_{x0} a_{y0}}}\sqrt{\frac{q_{x0}}{q_x(L)}}\sqrt{\frac{q_{y0}}{q_y(L)}}\exp(jkL)\exp\left[jkx_2^2/2q_x(L)\right]\exp\left[jky_2^2/2q_y(L)\right] \\ &= \sqrt{\frac{P_t}{\pi a_x(L) a_y(L)}}\exp\left[jkL + \{\Theta_x(L)+\Theta_y(L)\}/2\right] \\ &\quad \times \exp\left[jkx_2^2/2q_x(L)\right]\exp\left[jky_2^2/2q_y(L)\right] \qquad (16.25)\end{aligned}$$

with

$$\Theta_i = -\tan^{-1}\left(\frac{\Omega_{iL}^{-1}}{1+L/R_{i0}}\right), \qquad (16.26)$$

$$\Omega_{iL} = \frac{ka_{i0}^2}{L}, \qquad (16.27)$$

for $i = x, y$. Separating Eq. (16.24) into real and imaginary parts, one can also show that

$$a_i(L) = a_{i0}\left[(1+L/R_{i0})^2 + \Omega_{iL}^{-2}\right]^{1/2}. \qquad (16.28)$$

$$R_i(L) = L\frac{\left[(1+L/R_{i0})^2 + \Omega_{iL}^{-2}\right]}{\left[(1+L/R_{i0})L/R_{i0} + \Omega_{iL}^{-2}\right]}. \qquad (16.29)$$

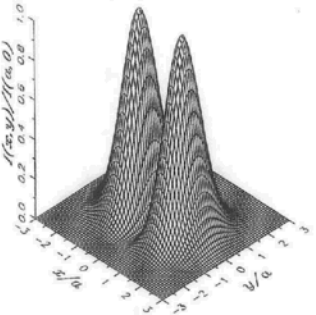

Figure 16.2: *Intensity profile of a TEM_{10} Gaussian beam.*

16.5 Higher-Order Gaussian Beams

Many optical systems can support higher-order Gaussian beams having the following transverse spatial dependence:

$$U_{\mathrm{TEM}_{nm}}(\vec{\rho}) = \left(\frac{P_t}{\pi a_0^2 n! m! 2^{n+m}}\right)^{1/2} H_n(x/a_0) H_m(y/a_0) \exp(jk|\vec{\rho}|^2/2q_0), \tag{16.30}$$

where H_n is the nth order Hermite polynomial, and the rest of the quantities are as defined before. Such a beam is referred to be in the TEM_{nm} (transverse electromagnetic) mode. A few of the lowest order Hermite polynomials are

$$H_0(x) = 1, \tag{16.31}$$

$$H_1(x) = 2x, \tag{16.32}$$

$$H_2(x) = 4x^2 - 2, \tag{16.33}$$

$$H_3(x) = 8x^3 - 12x. \tag{16.34}$$

The intensity profile associated with the TEM_{10} mode is

$$I_{\mathrm{TEM}_{10}}(\vec{\rho}) = \sqrt{\frac{2P_t}{\pi a_0^4}}\, x \exp(-|\vec{\rho}|^2/a_0^2). \tag{16.35}$$

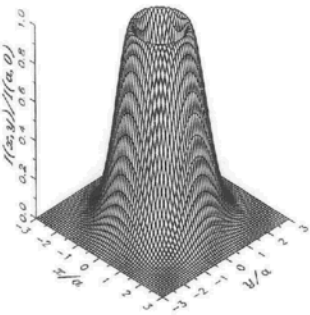

Figure 16.3: *Intensity profile of the donut-mode Gaussian beam.*

The x and y intensity dependences of the TEM_{10}mode are plotted in Fig. 16.2.

Under certain conditions, lasers can support what is known as the donut mode. It is a 50/50 superposition of the TEM_{01} and TEM_{10} modes with a $\pi/2$ phase shift. The transverse field dependence of the donut mode can be written as

$$U_{\mathrm{donut}}(\rho) = \frac{U_{10}(\bar{\rho}) \pm jU_{01}(\bar{\rho})}{\sqrt{2}}, \tag{16.36}$$

where either the + or the − sign can be chosen. Using transverse dependences of the TEM_{01} and TEM_{10} modes,

$$U_{\mathrm{donut}}(\bar{\rho}) = \sqrt{\frac{2P_t}{\pi a_0^4}} \frac{x \pm jy}{\sqrt{2}} \exp\left(jk|\bar{\rho}|^2/2q_0\right), \tag{16.37}$$

and the transverse intensity profile is given by

$$\begin{aligned} I_{\mathrm{donut}}(\bar{\rho}) &= |U_{\mathrm{donut}}(\bar{\rho})|^2 \\ &= \frac{P_t}{\pi a_0^4}\left(x^2+y^2\right)\exp\left(-|\bar{\rho}|^2/a_0^2\right), \end{aligned} \tag{16.38}$$

which is plotted in Fig. 16.3 as a function of both x and y.

NORTHWESTERN UNIVERSITY
Department of Electrical Engineering and Computer Science

Lecture 17 – EECS 379

PROPAGATION OF GAUSSIAN BEAMS: A FEW EXAMPLES

Reading Assignment: YARIV – Secs. 2.4 and 2.5.

17.1 Introduction

We have shown in the previous lecture that Gaussian beams maintain their form as they propagate through free space. Only the complex parameter q, describing their intensity radius a and the phase radius of curvature R, changes according to

$$q(z) = q_0 + z, \tag{17.1}$$

where q_0 is the initial value at $z = 0$. Thus in Gaussian-beam propagation problems, it is enough to track the behavior of $q(z)$, or of the components $R(z)$ and $a(z)$, from place to place. If needed, the spatial profile of the complex envelope $U_z(\bar{\rho})$ describing the Gaussian beam at any z can be obtained immediately from Eq. (16.2); it is given by

$$U_z(\bar{\rho}) = \sqrt{\frac{P_t}{\pi a^2(z)}}\, \exp[jkz + j\Theta(z)] \exp[jk|\bar{\rho}|^2/2q(z)], \tag{17.2}$$

where

$$\Theta(z) = -\tan^{-1}[\Omega_z^{-1}/(1 + z/R_0)], \tag{17.3}$$

$$\Omega_z = \frac{ka_0^2}{z}. \tag{17.4}$$

Below we consider a few examples that commonly arise in various applications of Gaussian beams.

17.2 Collimated Gaussian Beam

The first example we consider is that of a beam which is collimated at $z = 0$, i.e., its phase-fronts are parallel and flat with an infinite radius of curvature. Substituting $R_0 = \infty$ in

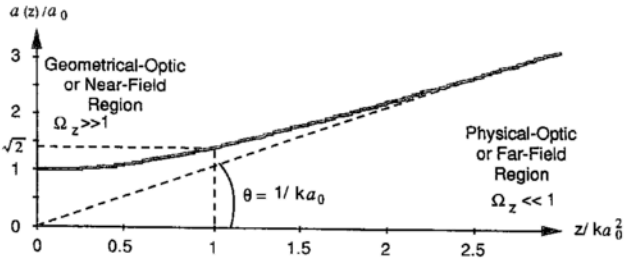

Figure 17.1: *Intensity radius of an initially collimated Gaussian beam.*

Eqs. (16.13) and (16.12), the intensity radius and the phase radius of curvature are given by

$$a(z) = a_0[1+\Omega_z^{-2}]^{1/2} = a_0\sqrt{1+\frac{z^2}{k^2a_0^4}}, \tag{17.5}$$

$$R(z) = z[1+\Omega_z^2] = z[1+\frac{k^2a_0^4}{z^2}]. \tag{17.6}$$

Let us now examine the behavior of $a(z)$ and $R(z)$, the first of which is plotted in Fig. 17.1. We have chosen to display the normalized intensity radius $a(z)/a_0$ versus the normalized distance $z/ka_0^2 = \Omega_z^{-1}$. We first notice that in the region for which $z \ll ka_0^2$ or $\Omega_z \gg 1$, $a(z) \simeq a_0$ and $R(z) \simeq k^2a_0^4/z = ka_0^2\Omega_z \gg 1$. We call this the geometrical optic region because in this region $a(z)$ and $R(z)$ do not deviate much from their initial values at $z = 0$. The Gaussian beam stays collimated and its phase-fronts stay flat. A collimated pencil of rays behaves this way in the geometrical-optic description of light.

We next investigate the region for which $z \gg ka_0^2$ or $\Omega_z \ll 1$. In this region, $a(z) \simeq a_0/\Omega_z = z/ka_0$, and $R(z) \simeq z$. We call this the physical-optic region because in this region the wave nature of the Gaussian beam really stands out. Both the intensity radius $a(z)$ and the phase radius of curvature $R(z)$ increase linearly with z. The behavior of the latter is the same as that for spherical waves emitted by a point source located at $z = 0$. The former implies that the paraxial intensity $P_t/\pi a^2(z)$ falls inversely as z^2 just as it would for

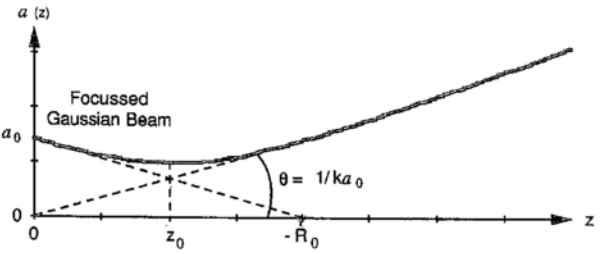

Figure 17.2: *Intensity radius of an initially focussed Gaussian beam.*

spherical waves emitted by a point source at $z = 0$. The transverse intensity profile, however, stays Gaussian at all z. In summary, in the region $z \gg ka_0^2$, the spreading Gaussian beam appears as if it was a right circular conical section out of spherical waves emitted by a point source located at $z = 0$. The half-angle of divergence θ is given by

$$\theta = \tan^{-1} \frac{a(z)}{z} = \tan^{-1} \frac{1}{ka_0} \simeq \frac{1}{ka_0} = \frac{\lambda}{2\pi a_0}. \tag{17.7}$$

As a numerical example, let us consider the Gaussian beam emitted by a He-Ne laser that you have seen in the laboratory. For such a beam $\lambda = 632.8$nm and a_0 is typically 0.5mm at the output mirror of the laser. The geometric region, also called the near-field region, for this beam extends to $ka_0^2 = 2\pi a_0^2/\lambda \simeq 2.5$m from the output mirror. $z \gg 2.5$m constitutes the physical-optic or the far-field region. The half-angle of divergence is $\theta = \lambda/2\pi a_0 \simeq 0.2$mrad.

17.3 Focussed Gaussian Beam

The second example we consider is that of a beam which has a negative radius of curvature $R_0 = -|R_0|$ at $z = 0$. From Eq. (16.13), the intensity radius for such a beam is given by

$$a(z) = a_0 \sqrt{(1 - \frac{z}{|R_0|})^2 + \Omega_z^{-2}}, \tag{17.8}$$

which is plotted in Fig. 17.2 for $z > 0$. Because the radius of curvature at $z = 0$ is negative, the Gaussian beam has converging wave fronts which give rise to a decreasing intensity radius

for $z > 0$. The beam comes to a focus, that is, it achieves a minimum intensity radius at some value of z, say z_0, and then spreads out. z_0 can be obtained by equating the derivative $\frac{d}{dz}a(z)$ or $\frac{d}{dz}a^2(z)$ equal to zero. We get

$$\begin{aligned}\frac{d}{dz}a^2(z) &= a_0^2\left[2\left(1-\frac{z}{|R_0|}\right)\left(\frac{-1}{|R_0|}\right)+\frac{2z}{(ka_0^2)^2}\right] \\ &= 0,\end{aligned}$$

which when solved gives

$$z_0 = \frac{|R_0|\Omega_0^2}{1+\Omega_0^2}, \tag{17.9}$$

where

$$\Omega_0 \equiv ka_0^2/|R_0| \tag{17.10}$$

is a dimensionless parameter. Substituting z_0 in Eq. (17.8), the minimum intensity radius $a(z_0)$ is found to be

$$\begin{aligned}a(z_0) &= a_0\sqrt{(1-\frac{\Omega_0^2}{1+\Omega_0^2})^2+\frac{|R_0|^2\Omega_0^4}{(1+\Omega_0^2)^2(ka_0^2)^2}} \\ &= \frac{a_0}{\sqrt{1+\Omega_0^2}}.\end{aligned} \tag{17.11}$$

Let us now interpret these results. First of all, we see from Eq. (17.9) that $z_0 < |R_0|$ implying that the minimum intensity radius, i.e., the *beam waist*, occurs before the value predicted by the initial radius of curvature. See Fig. (17.2). When $\Omega_0 \gg 1$ or $ka_0^2 \gg |R_0|$, we are in the so called geometrical-optic limit because then $z_0 \simeq |R_0|$ and $a(z_0) \simeq a_0/\Omega_0 \ll a_0$. These results are in agreement with the laws of geometrical optics according to which a converging beam with an initial radius of curvature $-|R_0|$ should come to a point focus at $z_0 = |R_0|$. On the other hand, when $\Omega_0 \ll 1$, i.e., $ka_0^2 \ll |R_0|$, $z_0 \simeq |R_0|\Omega_0^2$ and $a(z_0) \simeq a_0$ resulting in a large deviation from the geometrical-optic result. A focussed beam with $\Omega_0 \ll 1$ is dominated by the effects of diffraction. In this limit the initially negative radius of curvature fails to significantly decrease the initial intensity radius.

At a very large z ($z \gg z_0$), from Eq. (17.8), $a(z)$ is approximately given by

$$a(z) \simeq a_0\sqrt{\frac{z^2}{|R_0|^2}+\frac{z^2}{(ka_0^2)^2}}$$

$$= \frac{a_0 z}{k a_0^2}\sqrt{1+\Omega_0^2}. \qquad (17.12)$$

If $\Omega_0 \gg 1$, $a(z) \simeq a_0 z/|R_0|$ and the half-angle of divergence θ obeys the geometrical-optic result $\theta = \tan^{-1}[a(z)/z] = \tan^{-1}[a_0/|R_0|]$. On the other hand if $\Omega_0 \ll 1$, the behavior of the initially focussed Gaussian beam is not much different from that of an initially collimated beam. In this limit, the half-angle of divergence is given by $\theta = \tan^{-1}[a(z)/z] = \tan^{-1}(1/ka_0)$, which should be compared with Eq. (17.7).

The radius of curvature for an initially focussed Gaussian beam follows [cf. Eq. (16.12)]

$$R(z) = -z\,\frac{(1-z/|R_0|)^2+\Omega_z^{-2}}{z(1-z/|R_0|)/|R_0|-\Omega_z^{-2}}. \qquad (17.13)$$

It is easy to show that $R(z_0) = \infty$. Moreover, for $z < z_0$, $R(z) < 0$ and for $z > z_0$, $R(z) > 0$. [These results are readily obtained by noting the behavior of the denominator

$$\begin{aligned}\frac{z}{|R_0|}(1-\frac{z}{|R_0|}) - \Omega_z^{-2} &= \frac{z}{|R_0|} - \frac{z^2}{|R_0|^2} - \frac{z^2|R_0|^2}{|R_0|^2(ka_0^2)^2} \\ &= \frac{z}{|R_0|} - \frac{z^2}{|R_0|^2} - \frac{z^2}{|R_0|^2\Omega_0^2} \\ &= \frac{z}{|R_0|}(1-\frac{z}{z_0})\end{aligned}$$

in Eq. (17.13), where Eqs. (17.10) and (17.9) have been substituted.] Thus, the radius of curvature of the initially focussed Gaussian beam stays negative until the waist (the point of minimum intensity radius) at $z = z_0$ where it becomes infinite. The phase fronts at this point are parallel and flat. Thereafter, the radius of curvature becomes positive as it would be for a diverging beam.

17.4 Spherical Mirror Resonators

The simplistic theory of a laser that we considered in Lecture 8 was constructed for a laser resonator made of plane mirrors. In practice, however, most lasers use curved-mirror resonators which are easily analyzed using the Gaussian beam formalism. In fact, the lowest order natural modes of curved-mirror resonators have Gaussian transverse profiles.

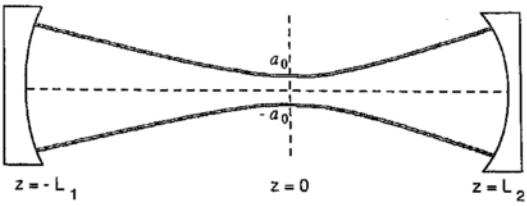

Figure 17.3: *Schematic of a curved-mirror resonator.*

Let us consider a Gaussian beam with a waist of radius a_0 at $z = 0$ as shown in Fig. 17.3. As the beam propagates to the right, its intensity radius and the phase radius of curvature change according to Eqs. (17.5) and (17.6). We let the beam propagate up to $z = L_2$ where we place a mirror of diameter d_2 and radius of curvature R_2. If we choose $d_2 > 4a(L_2)$, $R_2 = R(L_2)$, and orient the mirror perpendicular to the optical axis (z axis), then the Gaussian beam would be reflected upon itself and propagate along the $-z$ direction retracing its path through $z = 0$. Now we let the beam propagate to the left up to $z = -L_1$ and place another mirror of diameter d_1 and radius of curvature R_1 perpendicular to the optical axis. Since both Eqs. (17.5) and (17.6) are even functions of z, they apply as well to the left propagating Gaussian beam as they do to the right propagating beam. Now if we choose $d_1 > 4a(-L_1)$ and $R_1 = R(-L_1)$, the Gaussian beam would be reflected upon itself once again and start bouncing back and forth between the two mirrors.

The situation here is similar to the plane-mirror Fabry-Perot resonator considered in Sec. 4.5. The resonance condition occurs when the phase shift due to one round-trip propagation equals an integral multiple of 2π. From Eq. (17.2)

$$\delta = 2[k(L_1 + L_2) + \Theta(L_1 + L_2)], \tag{17.14}$$

where $\Theta(L_1 + L_2)$ is obtained from Eq. (17.3) to be

$$\Theta(L_1 + L_2) = -\tan^{-1}\left[\frac{(L_1 + L_2)/ka^2(-L_1)}{1 + (L_1 + L_2)/R(-L_1)}\right]. \tag{17.15}$$

Setting $\delta = 2m\pi$, the mth resonance frequency is given by

$$\begin{aligned} \nu_m &= \frac{mc}{2(L_1+L_2)} - \frac{c\Theta(L_1+L_2)}{2\pi(L_1+L_2)} \\ &= \frac{mc}{2\ell} - \frac{c\Theta(\ell)}{2\pi\ell}, \end{aligned} \tag{17.16}$$

and the free-spectral range (FSR) is $\Delta\nu = c/2\ell$, where $\ell \equiv L_1 + L_2$. Thus, we see that the usage of curved mirrors leaves the FSR unchanged whereas the absolute resonance frequency ν_m is modified [cf. Eqs. (4.15) and (4.14) with $\theta_T = 0$ and $n = 1$]. Since the transverse profile of a Gaussian beam extends to infinity, there is some diffraction loss at each mirror. By choosing the mirrors large enough [$d_1 > 4a(-L_1)$ and $d_2 > 4a(L_2)$], this loss can be minimized to any desired value. Such a choice is not available with plane mirror resonators.